Recent Ice Ages on Mars: The Role of Radiatively Active Clouds and Cloud Microphysics

J.-B. Madeleine [1,2,3], J. W. Head [1], F. Forget [3], T. Navarro [3], E. Millour [3],
A. Spiga [2,3], A. Colaïtis [3], A. Määttänen [4], F. Montmessin [4], J. L. Dickson [1]
[1] Department of Geological Sciences, Brown University, Providence, USA
[2] Sorbonne Universités, UPMC Univ Paris 06, UMR 8539, Laboratoire de Météorologie Dynamique (IPSL), F-75005, Paris, France
[3] CNRS, UMR 8539, Laboratoire de Météorologie Dynamique (IPSL), F-75005, Paris, France
[4] LATMOS, CNRS/UVSQ/IPSL, Guyancourt, France

Global Climate Models (GCMs) have been successfully employed to explain the origin of many glacial deposits on Mars. However, the Latitude Dependent Mantle (LDM), a dust-ice mantling deposit that is thought to represent a recent "Ice Age", remains poorly explained by GCMs. We re-examine this question by considering the effect of radiatively active water-ice clouds (RACs) and cloud microphysics. We find that when obliquity is set to $35°$, as often occurred in the past 2 million years, warming of the atmosphere and polar caps by clouds modifies the water cycle and leads to the formation of a several centimeter-thick ice mantle poleward of $30°$ in each hemisphere during winter. This mantle can be preserved over the summer if increased atmospheric dust content obscures the surface and provides dust nuclei to low-altitude clouds. We outline a scenario for its deposition and preservation that compares favorably with the characteristics of the LDM.

1. Introduction

Multiple lines of evidence have been documented for surface deposits that formed as a result of recent quasi-periodic climate change on Mars [*Kreslavsky and Head*, 2000; *Mustard et al.*, 2001; *Boynton et al.*, 2002; *Dickson and Head*, 2009; *Levy et al.*, 2010, and images therein]. These data all pointed to the presence of a succession of meters-thick, latitude dependent surface deposits that are geologically young, found poleward of $30°$ in each hemisphere and ice-rich when formed [*Head et al.*, 2003]. Latitude is the single variable with which all of these diverse observations correlate, and climate is the only process known to be latitude-dependent. All of these factors provide compelling evidence for climate-driven water ice and dust mobility and emplacement during the recent period of higher obliquity. These observations were interpreted to represent ice ages [*Head et al.*, 2003], during which deposition and removal of mixtures of dust and water ice were controlled by climate variations resulting from quasi-periodic variation in orbital and spin-axis parameters. In this scenario [*Head et al.*, 2003], meters of ice and dust would have been deposited in the past millions of years to form a Latitude Dependent Mantle (LDM) and, as obliquity changed, surface ice stability zones shrank toward the polar caps, creating a latitude-dependent sublimation of ice from the uppermost ice mantle, and forming a protective dust

lag over the remaining ice. In the recent interglacial period ($\sim$0.4 Ma until the present), obliquity variations damped down, surface ice stability zones migrated to higher latitudes [*Schorghofer and Forget*, 2012], and the mid-latitude zone underwent preferential sublimation of ice, causing desiccation and pitting [*Milliken et al.*, 2003] of these layered deposits.

Assuming the same climate system and initial ice reservoirs (polar caps) as on present-day Mars, but assuming higher obliquities, a first generation of GCMs (including a simple representation of the water cycle) predicted the formation of perennial ice deposits in the tropics when the obliquity is above about $40°$ [*Mischna et al.*, 2003; *Levrard et al.*, 2004; *Forget et al.*, 2006]. These simulations have been useful to interpret the origin of observed tropical and mid-latitude glacier-like structures [*Head and Marchant*, 2003], but could not simply explain the link between obliquity increase and formation of the LDM. Nevertheless, *Levrard et al.* [2004] showed that when Mars returns to lower obliquity conditions after an excursion at high obliquity, the low and mid-latitude glaciers formed at high obliquity become unstable, water ice partially sublimes and tends to accumulate in both hemispheres above $60°$ latitude. However, these simulations are not in complete agreement with the geological record: the perennial ice cover does not extend to $30°$ latitude and the need for a tropical water source to form the LDM (estimated to be a few million years old at most) seems to be inconsistent with the estimated age of the tropical glaciers [*Head and Marchant*, 2003; *Shean et al.*, 2007].

Subsequent to that time, new observations and modeling work emphasized the importance of Radiatively Active Clouds [RACs, *Hinson and Wilson*, 2004; *Wilson et al.*, 2008; *Madeleine et al.*, 2012] and cloud microphysics [*Michelangeli et al.*, 1993; *Montmessin et al.*, 2002]. Given the impact of obliquity and orbital variations on the water cycle, we can expect these processes to play a critical role in recent climate history as well. Therefore, these processes have been implemented in the LMD/GCM as described in section 2, and we analyze in this paper their influence on recent ice ages. We show that the new results compare very well to the nature of the LDM, and we outline a new climate scenario for the recent ice ages on Mars.

2. The LMD Mars Global Climate Model

2.1. New physical processes

The version of the LMD/GCM used in this study is based on the model described in *Forget et al.* [1999] and *Montmessin et al.* [2004], to which has been added a set of new physical processes: a semi-interactive dust scheme [*Madeleine et al.*, 2011], a new cloud microphysics scheme [*Navarro et al.*, 2014], Radiatively Active Clouds [RACs,

Madeleine et al., 2012], a parameterization of the mixing by thermal plumes in the boundary layer [*Colaïtis et al.*, 2013], and the ice-thermal inertia feedback [*Madeleine et al.*, 2009].

Compared to previously published paleoclimate simulations [e.g. *Levrard et al.*, 2004; *Forget et al.*, 2006; *Montmessin et al.*, 2007; *Madeleine et al.*, 2009], the dust cycle is still following a specified visible dust opacity τ_{dust}, but in a "semi-interactive" way. Instead of using an analytical dust profile [modified Conrath profile, see *Forget et al.*, 1999], we constrain the GCM to specified dust column averaged contents according to a given paleoclimatic scenario while at the same time simulating the transport to interactively compute the vertical distribution of the particles. This dust scheme is coupled to a new cloud microphysics scheme that accounts for nucleation and growth of water ice particles onto dust nuclei (with a constant contact parameter of 0.95) as well as scavenging of dust particles by clouds. The radiative effect of water-ice clouds is taken into account, and depends on the size of the particles [*Madeleine et al.*, 2012]. In order to avoid numerical instabilities due to short time-scale and large-amplitude variations in the infrared cloud opacity, an implicit calculation of the CO_2 15 μm band heating rates is performed following section 4a of *Dufresne et al.* [2005] with $\alpha = 1$ (implicit scheme).

2.2. Simulation setup

The ages of the LDM suggest that it was forming during the past five million years, at periods when the obliquity was ranging from 15° to 35°. Therefore, we ran a set of simulations summarized in Table 1 assuming either a north or south polar cap and an obliquity in the 15–35° range. The simulations have a resolution of 32×24 grid points (Figures 2 and 1) or 64×48 grid points (Figure 3), with 29 vertical levels going up to 80 km. The polar caps are simulated by setting source points for latitudes poleward of ±80°. In order to accurately represent nucleation and cloud opacity in the model, a time-splitting method was introduced in the microphysics scheme by *Navarro et al.* [2014] and the same method is applied to the paleoclimate simulations presented here to make sure that clouds are correctly represented. The values of albedo and thermal inertia used for the polar caps are set to 0.35 and 800 J s$^{-1/2}$ m^{-2} K^{-1} respectively, based on present-day simulations validated against the TES (Thermal Emission Spectrometer) observations [see *Navarro et al.*, 2014]. When more than 5 μm of water ice

is deposited on the ground, the albedo is set to 0.35. The thermal inertia of the different subsurface layers is also set to 800 J s$^{-1/2}$ m^{-2} K^{-1} as ice accumulates [*Madeleine et al.*, 2009]. In order for equilibrium to be reached, the results shown are those of the sixth Martian year of simulation.

3. Results

3.1. Radiatively Active Clouds (RACs)

We start by analyzing the impact of RACs on the water cycle when the obliquity is either decreased or increased by 10° compared to the present-day value of ∼25°. The annual evolution of the water vapor (contoured) and cloud ice columns (shaded) are represented in the first row of Figure 2 for simulations x_{35}^*, x_{35} and $x_{35}^{S\downarrow}$. Table 1 gives the parameters used for these simulations and the predicted annual mean surface temperatures, water vapor columns and ice columns. Without RACs, an increase in the obliquity from 25° to 35° results in similar changes as those already described in the introduction as well as in *Mischna et al.* [2003], *Haberle et al.* [2003], *Levrard et al.* [2004], *Newman et al.* [2005], *Forget et al.* [2006] and *Madeleine et al.* [2009]. Summer insolation at the pole is increased, cap sublimation is intensified, and more water vapor is introduced into the atmosphere. In contrast, at low obliquity (15°), the atmosphere stays dry because of the low insolation over the polar caps (see Table 1), and ice remains at the poles. As mentioned in the introduction, the results of the low obliquity simulations performed by *Levrard et al.* [2004] were different because of the presence of water sources at the equator.

When the effect of RACs is taken into account, the response of the water cycle to an increase in obliquity is considerably amplified. When comparing two simulations without and with RACs (simulations x_{35}^* and x_{35}), an increase in the water vapor content of the atmosphere of more than an order of magnitude is found, as can be seen by comparing the contours of panels a and b of Figure 2. The global annual mean water vapor column rises from ∼40 pr.μm at 25° obliquity to almost 1900 pr.μm at 35° (see $\overline{q}_{vap}$ in Table 1; precipitable micrometers, or pr.μm, refer to the equivalent depth of a column of liquid water that would be produced by condensing out all the water vapor in the atmosphere). As discussed in *Hinson and Wilson* [2004], *Wilson et al.* [2008] and *Madeleine et al.* [2012], clouds have multiple effects on the martian climate and thermal structure of the atmosphere. By comparing simulations x_{35}^* and x_{35}, the net effect of RACs in the polar regions is found to correspond to a warming of the surface of ∼20 K by infrared emission

Table 1. Obliquity ϵ, eccentricity e, solar longitude of perihelion L$_p$, water-ice reservoirs WIR, dust opacity τ_{dust}, surface temperature $\overline{T}_s$, water vapor column $\overline{q}_{vap}$, and ice column $\overline{q}_{ice}$ for the different simulations described in the paper. $\overline{T}_s$, $\overline{q}_{vap}$ and $\overline{q}_{ice}$ are global mean area-weighted values. RACs stands for Radiatively Active Clouds. $N \uparrow$ means that mantle formation is favored in the northern hemisphere, and conversely for $S \downarrow$ (see section 3.2). RACs are responsible for a 25 K increase in the mean surface temperature when the obliquity is increased from 25 to 35° (simulations x_{25} and x_{35}).

#	Scenarios					Results		
	ϵ ($^\circ$)	e	L$_p$ ($^\circ$)	WIR	τ_{dust}	$\overline{T}_s$ (K)	$\overline{q}_{vap}$ (pr.μm)	$\overline{q}_{ice}$ (pr.μm)
x_{15}	15	0		NPC	0.2	205.9	0.058	0.0014
x_{25}	25	0		NPC	0.2	213.4	38.6	9.9
x_{35}^*	35	0		NPC	0.2	202.0	41.0	4.0
x_{35}	35	0		NPC	0.2	238.9	1874.5	296.6
$x_{35}^{S\downarrow}$	35	0.1	90	NPC	[0.2–2]	232.4	1142.4	144.7
$x_{35}^{N\uparrow}$	35	0.1	270	SPC	[0.2–2]	230.4	874.7	109.5

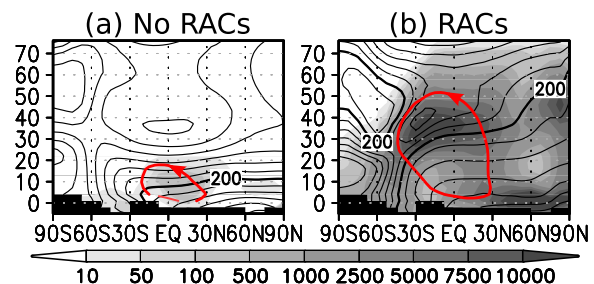* For this simulation, RACs are turned off.

Figure 1. Zonal mean temperature (contoured with an interval of 10 K) and cloud ice mole mixing ratio (shaded, ppm) during northern summer (L$_s$ = 60–90°) for simulations x_{35}^* (a) and x_{35} (b). The 5×10^9 kg s^{-1} contour of the stream function is also represented in red. Y-axis is altitude in km.
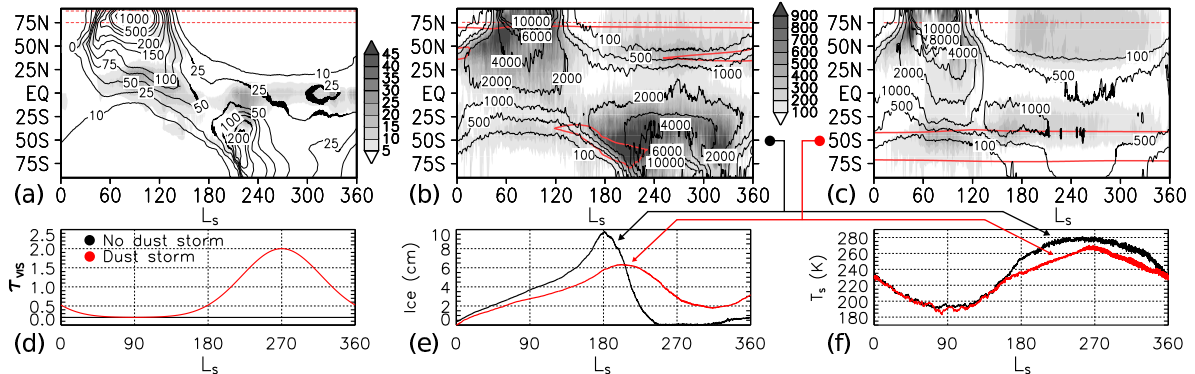
Figure 2. (a) Annual evolution of the water vapor column (contoured, pr.μm) and water ice column (shaded, pr.μm) as a function of L_s for simulation x_{35}^*. (b) Same as (a) for simulation x_{35}. (c) Same as (a) for simulation $x_{35}^{S\downarrow}$. The parameters used for these simulations are listed in Table 1. The dashed red line indicates regions of net sublimation, whereas the solid red line shows the regions where more than 5 cm of ice is present on the surface. (d) Globally specified dust optical depth at a reference pressure of 610 Pa in simulations x_{35} (black) and $x_{35}^{S\downarrow}$ (red). (e) Annual evolution of the zonal mean surface ice thickness at 50°S for simulation x_{35} (black) and $x_{35}^{S\downarrow}$ (red). (f) Same as (e) for daily mean surface temperature (K).

from clouds [an effect that is also observed in the tropics at night on present-day Mars, see *Wilson et al.*, 2007]. Consequently, the amount of ice that is sublimated from the north polar cap when clouds are active is around ten times that sublimated when clouds are not active.

In the simulation that includes RACs, the atmosphere is also warmed on average by cloud absorption of both solar radiation and infrared radiation emitted by the surface. An increase in the annual mean atmospheric temperature of $\sim$50 K is therefore simulated in the tropics at an altitude of $\sim$20 km when comparing simulation x_{35}^* to simulation x_{35}. This net warming results from the net effect of clouds that can otherwise cool or warm the atmosphere or surface depending on the specific region and time period [*Madeleine et al.*, 2012]. This warming is apparent when comparing panels a and b of Figure 1 where the zonal mean temperatures during northern summer are contoured for the two simulations. It increases the meridional temperature gradient and enhances the meridional circulation [as was the case in *Madeleine et al.*, 2012], which favors the mixing of water vapor. This is also shown in Figure 1 where the 5×10^9 kg s^{-1} contour of the stream function is represented in red and illustrates the latitudinal and vertical extension of the Hadley cell due to RACs. The changes in the thermal structure of the atmosphere when clouds are active result from a sharp increase in the amount of water-ice clouds that is apparent when comparing panels a and b of Figure 2. This increase in the cloud content is also apparent on Figure 1, where the cloud ice mole mixing ratio (shaded, ppm) is around two order of magnitude higher when clouds are active (see also $\overline{q}_{ice}$ in Table 1). By their own radiative effect, clouds warm the atmosphere, increase the water vapor holding capacity of the atmosphere, become even more opaque and trigger an efficient positive feedback loop. The result is a glacial climate that is significantly warmer and more humid than the present interglacial.

The impact of this increased cloud cover on surface water ice is significant. When clouds are not active, the atmosphere is drier (see $\overline{q}_{vap}$ in Table 1), and even though a seasonal ice layer forms in the winter hemisphere, its thickness at 50° latitude (which is later used as a reference in both hemispheres) does not exceed one millimeter. When clouds are active, the zonal mean ice thickness at 50° latitude almost reaches 10 cm (see Figure 2e, black). This mantle is entirely formed by precipitation from clouds, direct condensation of water vapor on the surface being only predicted at the poles. When clouds are not active, the atmosphere holds

less water vapor, and the precipitation rates in ice-covered regions are of the order of 2 micrometers per day. When clouds are active, the atmosphere is warmed on average and holds more water vapor, which results in ice precipitation rates of around one hundred micrometers per day.

Precipitation comes from a cloud belt that forms in the 30–50° latitude band, at the margin of the polar hood, and which has a water ice column of $\sim$250 pr.μm. This cloud belt can be seen in Figure 2b, around 50°S during southern winter ($L_s = 30$– 120°), and extends to the north pole during northern winter ($L_s = 210$–300°). Water is provided by the subsiding branch of the Hadley cell, and clouds form along the winter jet, as can be seen in Figure 1b. The deflection of the jet, strongly controlled by stationary planetary waves, results in a longitudinally uneven cloud belt, and thereby forms an equally uneven mantle. This several centimeter-thick mantle extends down to 30° in both hemispheres, in agreement with the observed LDM. During summer however, the mantle becomes unstable and sublimates away. The global net effect of RACs is indeed a warming of the atmosphere but also of the surface by a strong greenhouse effect. This large increase in surface temperature due to RACs is evident in Table 1. In order for the mantle to be preserved, another process needs to be invoked.

3.2. Coupling between the dust and water cycles

As discussed in the previous section, summer temperatures are too high to allow preservation of the mantle, which would undergo sublimation. Right after southern spring equinox, surface temperature at 50°S reaches more than 260 K (Figure 2f, black), and ice starts to sublimate (Figure 2e, black). To further explore the sensitivity of the mantle to climate conditions, we ran simulations $x_{35}^{N\uparrow}$ and $x_{35}^{S\downarrow}$, where the atmospheric dust content varies over the year in a similar manner as today's dust content. To do so, we simply used a Gaussian function whose minimum and maximum are located 180° of L_s apart and equal to $\tau_{dust} = 0.2$ and 2, respectively (see Figure 2d). In simulation $x_{35}^{S\downarrow}$, the conditions were chosen to favor the preservation of a mantle in the southern hemisphere by taking into account the effect of climatic precession, which has a period of about 51 kyr [*Laskar et al.*, 2002]. To do so, the eccentricity of the orbit was set to 0.1, the solar longitude of perihelion L_p was set to 90°, and the L_s of the dust opacity maximum was set to

270°. A polar cap (source of water vapor) was also introduced at the north pole. This configuration favors a high sublimation of the cap during northern summer when the planet is closest to the Sun and a reduced insolation during southern summer to preserve the mantle. The timing of the peak in dust opacity is also chosen to reduce the amount of sunlight reaching the surface during southern summer. The opposite conditions (i.e. a south polar cap, $L_p = 270°$ and dust peak at $L_s = 90°$) were set up for simulation $x_{35}^{N\uparrow}$ to favor the formation of a mantle in the northern hemisphere.

The water cycle for simulation $x_{35}^{S\downarrow}$ is represented in Figure 2c. The red contours in Figures 2b and 2c give an indication of the sublimation and accumulation of ice on the surface. When the atmosphere is not dusty during southern summer, more than 5 cm of ice is present on the surface around the equinox (see the red contour around 60°S after $L_s = 120°$ in Figure 2b), but these deposits are sublimated before the summer solstice. They do not sublimate during a dusty southern summer. In this case, the mantle is preserved (see the red contours at 40 and 70°S in Figure 2c) due to a decrease in the surface temperature both at night and day which is shown in Figure 2f (in red). During the day, the lower temperature is due to the obscuration of the surface induced by the higher dust optical depth. During the night, surface temperature is dominantly controlled by a low-altitude cloud layer that forms by condensation of the water vapor released by the mantle during the day. This cloud layer extends from the surface to an altitude of ~10 km and produces a warming of the lower atmosphere and surface by absorption and emission of infrared radiation. Increasing the dust optical depth in simulation $x_{35}^{S\downarrow}$ also results in more dust nuclei to condense onto in the lower atmosphere, resulting in a shallower cloud layer whose top altitude is reduced by up to 5 km compared to non-dusty conditions (x_{35}). Due to the lower vertical extent of this optically thick layer of clouds, nighttime atmospheric and surface temperatures are reduced by up to 20 K. This response of the model is made possible by the new microphysics scheme, which better represents the coupling between dust particles and cloud formation. After $L_s = 180°$, the rise in surface temperature is sufficiently reduced to allow preservation of ~2 cm of additional ice each year (see Figure 2e and f, in red).

The ice accumulation rates simulated by the GCM for simulations $x_{35}^{N\uparrow}$ and $x_{35}^{S\downarrow}$ are represented in Figure 3. In the northern hemisphere (panel a), ~2 cm of ice is deposited every year down to a latitude of ~45°. The spatial distribution is in good agreement with the diffuse roughness boundary (blue dotted line), which is consistent with the presence of the LDM [Kreslavsky and Head, 2000]. If the polar cap, L_s of perihelion and dust cycle are changed to favor deposition in the southern hemisphere (panel b), the GCM results agree with the geology only between 90 and 240°E. Outside this longitudinal band, the observed LDM extends closer to the equator and down to a latitude of ~30°S, whereas the GCM mantle reaches this latitude only seasonally (red line).

The formation of the mantle was thus possible under the conditions of the ~2.1–0.4 Ma period and appears to be extremely sensitive to the dust cycle. Simulations $x_{35}^{N\uparrow}$ and $x_{35}^{S\downarrow}$ are only part of a wider range of conditions under which the mantle can form but probably at a more moderate pace. We also assessed the sensitivity of these simulations to the model parameters (introduced in sections 2.1 and 2.2), especially the ice albedo and thermal inertia which probably varied in the past. We found that the net accumulation rates can be modulated by the resulting change in the sublimation of the polar caps (north or south), and the mantle accumulation can even stop for relatively high values of albedo and thermal inertia (~0.5 and 1500 J s$^{-1/2}$ m^{-2} K^{-1}, respectively). Moreover, when the polar cap is exposed and sublimates, a dust lag might cover the ice and decrease sublimation. In simulation $x_{35}^{S\downarrow}$, the cap loses tens of centimeters of ice every year. In this case, a dust lag would also limit the amount of water vapor provided by the cap, an effect that we do not yet take into account.

4. Application to recent Mars history

Our results allow us to revisit the recent history of Mars. Using the data from *Laskar et al.* [2004], we can determine that conditions close to simulations $x_{35}^{N\uparrow}$ and $x_{35}^{S\downarrow}$ happened multiple times over the last 2.1 million years for about one thousand years each time. Due to the increased obliquity and influence of Radiatively Active Clouds (RACs), surface warming favored sublimation of the polar caps, whereas atmospheric warming increased water vapor holding capacity, strengthened the meridional circulation by up to a factor of 2, and formed a cloud belt in the 30–50° latitude band of both winter hemispheres. Each year, this all resulted in the deposition of a several centimeter-thick ice seasonal mantle poleward of 30° in both hemispheres. If we assume that during these excursions, climate processes such as the dust storms prescribed in simulations $x_{35}^{N\uparrow}$ and $x_{35}^{S\downarrow}$ occurred every year, then the mantle can be preserved and an upper estimate of ten meters of ice was accumulated during each of these excursions.

When the obliquity started to decline, the atmosphere became dry again, and part of the mantle sublimated away. The new microphysics scheme allows us to quantify the amount of dust that is scavenged by clouds and embedded within the ice deposits. The simulated mantle is made of up to 5 wt% of scavenged dust particles, assuming that these dust particles are not remobilized by wind. If we assume that a few centimeters of dust particles are necessary to protect the mantle from sublimating [*Schorghofer*, 2010], then more than a meter of ice must be sublimated to generate a sufficiently thick dust cover. Recent obliquity cycles would result, in this case, in the formation of a succession of meters-thick layers made of relatively pure ice and topped by a layer of dust particles of a few centimeters.
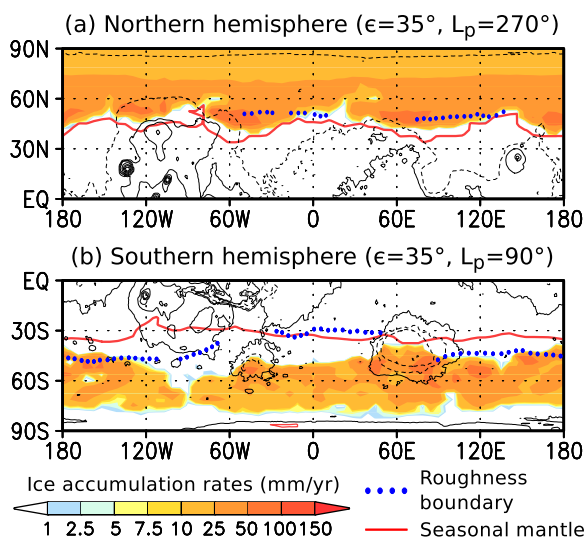

Figure 3. Annual ice accumulation rates (mm/yr) for simulation $x_{35}^{N\uparrow}$ (a) and $x_{35}^{S\downarrow}$ (b). The boundary of the Latitude Dependent Mantle (LDM) is indicated by the blue dotted line, based on the roughness map of *Kreslavsky and Head* [2000]. The red line shows the 1 cm contour of the annual maximum ice thickness.

The mantle spatial distribution simulated by the GCM and the assessment of its thickness and stratigraphy based on our results are, to first order, consistent with the observed properties of the LDM [*Head et al.*, 2003] and suggest that the mantle is indeed recent and formed in the last few million years. This study underlines the key role of radiatively active clouds in the recent climate history of Mars and the sensitivity of the whole climate to the dust cycle and cloud microphysical properties.

Acknowledgments

References

Boynton, W. V., et al., Distribution of Hydrogen in the Near Surface of Mars: Evidence for Subsurface Ice Deposits, *Science*, *297*, 81–85, 2002.

Colaïtis, A., A. Spiga, F. Hourdin, C. Rio, F. Forget, and E. Millour, A thermal plume model for the Martian convective boundary layer, *Journal of Geophysical Research (Planets)*, *118*, 1468–1487, doi:10.1002/jgre.20104, 2013.

Dickson, J. L., and J. W. Head, The formation and evolution of youthful gullies on Mars: Gullies as the late-stage phase of Mars most recent ice age, *Icarus*, *204*, 63–86, doi: 10.1016/j.icarus.2009.06.018, 2009.

Dufresne, J.-L., R. Fournier, C. Hourdin, and F. Hourdin, Net Exchange Reformulation of Radiative Transfer in the CO_2 15-μm Band on Mars., *Journal of Atmospheric Sciences*, *62*, 3303–3319, doi:10.1175/JAS3537.1, 2005.

Forget, F., F. Hourdin, R. Fournier, C. Hourdin, O. Talagrand, M. Collins, S. R. Lewis, P. L. Read, and J.-P. Huot, Improved general circulation models of the Martian atmosphere from the surface to above 80 km, *Journal of Geophysical Research*, *104*, 24,155–24,176, 1999.

Forget, F., R. M. Haberle, F. Montmessin, B. Levrard, and J. W. Head, Formation of Glaciers on Mars by Atmospheric Precipitation at High Obliquity, *Science*, *311*, 368–371, 2006.

Haberle, R. M., J. R. Murphy, and J. Schaeffer, Orbital change experiments with a Mars general circulation model, *Icarus*, *161*, 66–89, 2003.

Head, J. W., and D. R. Marchant, Cold-based mountain glaciers on Mars; western Arsia Mons, *Geology*, *31*(7), 641–644, 2003.

Head, J. W., J. F. Mustard, M. A. Kreslavsky, R. E. Milliken, and D. R. Marchant, Recent ice ages on Mars, *Nature*, *426*, 797–802, 2003.

Hinson, D. P., and R. J. Wilson, Temperature inversions, thermal tides, and water ice clouds in the Martian tropics, *Journal of Geophysical Research (Planets)*, *109*, 1002–+, 2004.

Kreslavsky, M. A., and J. W. Head, Kilometer-scale roughness of Mars: Results from MOLA data analysis, *Journal of Geophysical Research*, *105*, 26,695–26,712, 2000.

Laskar, J., B. Levrard, and J. F. Mustard, Orbital forcing of the martian polar layered deposits, *Nature*, *419*, 375–377, 2002.

Laskar, J., A. C. M. Correia, M. Gastineau, F. Joutel, B. Levrard, and P. Robutel, Long term evolution and chaotic diffusion of the insolation quantities of Mars, *Icarus*, *170*, 343–364, 2004.

Levrard, B., F. Forget, F. Montmessin, and J. Laskar, Recent ice-rich deposits formed at high latitudes on Mars by sublimation of unstable equatorial ice during low obliquity, *Nature*, *431*, 1072–1075, 2004.

Levy, J. S., D. R. Marchant, and J. W. Head, Thermal contraction crack polygons on Mars: A synthesis from HiRISE, Phoenix, and terrestrial analog studies, *Icarus*, *206*, 229–252, doi:10.1016/j.icarus.2009.09.005, 2010.

Madeleine, J.-B., F. Forget, J. W. Head, B. Levrard, F. Montmessin, and E. Millour, Amazonian northern mid-latitude glaciation on Mars: A proposed climate scenario, *Icarus*, *203*, 390–405, doi:10.1016/j.icarus.2009.04.037, 2009.

Madeleine, J.-B., F. Forget, E. Millour, L. Montabone, and M. J. Wolff, Revisiting the radiative impact of dust on Mars using the LMD Global Climate Model, *Journal of Geophysical Research (Planets)*, *116*, E11010, doi:10.1029/2011JE003855, 2011.

Madeleine, J.-B., F. Forget, E. Millour, T. Navarro, and A. Spiga, The influence of radiatively active water ice clouds on the Martian climate, *Geophysical Research Letters*, *39*, L23,202, 2012.

Michelangeli, D. V., O. B. Toon, R. M. Haberle, and J. B. Pollack, Numerical simulations of the formation and evolution of water ice clouds in the Martian atmosphere, *Icarus*, *102*, 261–285, doi:10.1006/icar.1993.1048, 1993.

Milliken, R. E., J. F. Mustard, and D. L. Goldsby, Viscous flow features on the surface of Mars: Observations from high-resolution Mars Orbiter Camera (MOC) images, *Journal of Geophysical Research (Planets)*, *108*, 5057, doi: 10.1029/2002JE002005, 2003.

Mischna, M. A., M. I. Richardson, R. J. Wilson, and D. J. McCleese, On the orbital forcing of Martian water and CO_2 cycles: A general circulation model study with simplified volatile schemes, *Journal of Geophysical Research (Planets)*, *108*, 16–1, 2003.

Montmessin, F., P. Rannou, and M. Cabane, New insights into Martian dust distribution and water-ice cloud microphysics, *Journal of Geophysical Research (Planets)*, *107*, 4–1, 2002.

Montmessin, F., F. Forget, P. Rannou, M. Cabane, and R. M. Haberle, Origin and role of water ice clouds in the Martian water cycle as inferred from a general circulation model, *Journal of Geophysical Research (Planets)*, *109*, E10,004, 2004.

Montmessin, F., R. M. Haberle, F. Forget, Y. Langevin, R. T. Clancy, and J.-P. Bibring, On the origin of perennial water ice at the south pole of Mars: A precession-controlled mechanism?, *Journal of Geophysical Research (Planets)*, *112*, E08S17, 2007.

Mustard, J. F., C. D. Cooper, and M. K. Rifkin, Evidence for recent climate change on Mars from the identification of youthful near-surface ground ice, *Nature*, *412*, 411–414, 2001.

Navarro, T., J.-B. Madeleine, F. Forget, A. Spiga, E. Millour, F. Montmessin, and A. Määttänen, Global Climate Modeling of the Martian water cycle with improved microphysics and radiatively active water ice clouds, *Journal of Geophysical Research (Planets)*, doi:10.1002/2013JE004550, 2014.

Newman, C. E., S. R. Lewis, and P. L. Read, The atmospheric circulation and dust activity in different orbital epochs on Mars, *Icarus*, *174*, 135–160, 2005.

Schorghofer, N., Fast numerical method for growth and retreat of subsurface ice on Mars, *Icarus*, *208*, 598–607, doi: 10.1016/j.icarus.2010.03.022, 2010.

Schorghofer, N., and F. Forget, History and anatomy of subsurface ice on Mars, *Icarus*, *220*, 1112–1120, doi: 10.1016/j.icarus.2012.07.003, 2012.

Shean, D. E., J. W. Head, J. L. Fastook, and D. R. Marchant, Recent glaciation at high elevations on Arsia Mons, Mars: Implications for the formation and evolution of large tropical mountain glaciers, *Journal of Geophysical Research (Planets)*, *112*, E03,004, 2007.

Wilson, R. J., G. A. Neumann, and M. D. Smith, Diurnal variation and radiative influence of Martian water ice clouds, *Geophysical Research Letters*, *34*, L02,710, 2007.

Wilson, R. J., S. R. Lewis, L. Montabone, and M. D. Smith, Influence of water ice clouds on Martian tropical atmospheric temperatures, *Geophysical Research Letters*, *35*, 2008.